ECS | The Electrochemical Society
Advancing solid state & electrochemical science & technology

Facile and Scalable Electrochemical Synthesis of Ta-Nb Alloy Powders for Capacitors

View the article online for updates and enhancements.

CrossMark

Facile and Scalable Electrochemical Synthesis of Ta-Nb Alloy Powders for Capacitors

D. Sri Maha Vishnu,[1,2,z] Jagadeesh Sure,[1,2,a] Hyun-Kyung Kim,[3] and Carsten Schwandt[1,2,*]

[1]*Department of Materials Science and Metallurgy, University of Nizwa, 616 Nizwa, Sultanate of Oman*
[2]*Department of Materials Science and Metallurgy, University of Cambridge, Cambridge CB3 0FS, United Kingdom*
[3]*Gwangju Bio/Energy R&D Center, Korea Institute of Energy Research, Gwangju 61003, Republic of Korea*

The cost of tantalum (Ta), and thus of Ta capacitors, is undesirably high owing to the limited availability of its ores and the energy-intensive production. Reported herein is the economically viable electrochemical synthesis of Ta-Nb alloys as a potential replacement for Ta in capacitors. Ta-xNb (x = 20, 50, 80) alloys were prepared directly by electro-deoxidation of Ta_2O_5-Nb_2O_5 mixed oxide disks in $CaCl_2$ melt at 900 °C and the results were compared with those for the pure metals. The alloys and metals thus made were in the form of powders and consisted solely of the body-centered cubic phase. The overall compositions of the alloys were close to the target values. EDX and XPS analyses revealed that the particles underwent surface oxidation during the post-electrolytic washing process, thereby forming the required dielectric coating around the metallic cores. Cyclic voltammetry in an aqueous electrolytic cell demonstrated that all powders behaved as typical capacitor materials. TG/DSC studies on Ta and Ta-50Nb in air showed that oxidation commenced at 531 °C and 363 °C, respectively, with Ta-50Nb exhibiting an inversion in the temperature coefficient of the oxidation reaction at 650 °C. In overall, the method presented here for producing commercially relevant Ta-Nb alloys is both facile and scalable.

Ta and Nb belong to the refractory class of metals. These metals and their alloys possess extraordinary thermal and chemical stability, even to highly reactive concentrated acids.[1–3] Ta-Nb alloys also exhibit low-temperature superconductivity[4] and excellent biocompatibility.[5] Ta readily forms a thin protective film of surface oxide when in contact with the ambient atmosphere,[6] and Ta powder is widely employed for the production of electrolytic capacitors because the dielectric properties of this film around the metallic core endow it with high specific capacitance.[7] Commercial Ta capacitors typically comprise an anode of vacuum-sintered Ta, a dielectric layer of Ta_2O_5 on the Ta surface, and a cathode. They are classified into solid, wet and polymer types, depending on whether the cathode is MnO_2, a conducting liquid or a conducting polymer. The widespread usage of Ta capacitors is consequent of their exceptional volumetric and gravimetric efficiencies (expressed as *CV*/cm^3 and *CV*/g, where *C* and *V* are capacitance and applied voltage), their excellent stability over a wide range of frequencies and temperatures, and their long-term reliability.[8] More than 60% of all Ta produced is presently utilized for the manufacture of capacitors[9] for the automotive, aviation, military, electronics, computer, telecommunication, and medical sectors.[8]

Ta is known for its high and notoriously fluctuating price, which is caused by the limited availability of Ta ores, their occurrence in politically unstable regions, and the complex and expensive extraction and processing,[9,10] all of which directly affects the capacitor industry. Many alternative metals, including Al, Zr and Hf, have been researched for use as more viable capacitor materials but, other than Al that has gained some market share, none of them stood as a competitor to Ta.[7] Ta's sister element Nb is comparatively cheaper and its ores are more abundant.[10] Pure Nb metal powder has been trialed in the manufacture of capacitors but yielded comparatively lower working voltages and volumetric efficiencies as well as higher direct current leakage.[8] However, replacing a portion of the Ta with Nb without unacceptably compromising overall performance is considered feasible and would lower the cost of electrolytic

capacitors.[8] Nunes et al.[11] and Awasthi et al.[12] attempted the synthesis of Ta-Nb alloys via the co-reduction of the oxides by, respectively, Al and Si. However, like most other metallothermic reduction methods, this required excess amounts of reductant, gave low yields, and led to oxide inclusions. Furthermore, subsequent melting to homogenize the alloys provided a bulky and highly dense microstructure and necessitated hydriding-dehydriding as an additional process step to attain powders.[13]

Molten salt processes have traditionally played a key role in the production of several alkali and alkaline earth metals as well as Al. Notable progress, especially with respect to the winning of transition metals, has been achieved in recent years through the advent of the FFC process and the OS process. In the former process, an oxide cathode is reduced to the parent metal or alloy by polarization in a $CaCl_2$-based melt, such that oxide ions are expelled electrochemically from the cathode into the electrolyte without the electrolyte undergoing decomposition.[14–18] In the latter process, an oxide cathode is reduced by polarization in a $CaCl_2$-based melt, such that Ca metal from the electrolyte is deposited onto the oxide whereupon this is reduced chemically.[19,20] Both processes have been employed using $CaCl_2$- and also LiCl-based melts for the preparation of Ta[21–24] and Nb.[25–33] Alternatively, the production of Ta in molten salt was attempted through the simple addition of Ca metal to a chloride melt,[34] although this disadvantageously necessitated the handling of elemental Ca at elevated temperature. More recently, a new molten-salt process, derived from the FFC process and relying on the electro-reduction of an oxide cathode by Mg in a $MgCl_2$-based melt, has rendered possible the preparation of particularly fine Ta powder with an average particle size of only 50 nm.[35] It is further noted that our Group has reported a preliminary study into the production of Ta-54.5Nb alloy using a eutectic $CaCl_2$-NaCl melt[36] but this work has since not been pursued further.

This article communicates in detail the synthesis and characterization of Ta-xNb alloys (x = 20, 50, 80 mass%) in $CaCl_2$ melt at 900 °C and compares the key results with those of the preparation of Ta and Nb under the same conditions. Cyclic voltammetry in an aqueous electrolytic cell was employed to assess the electrochemical characteristics of the metallic powders made, and thermokinetic

*Electrochemical Society Member.
[a]Present address: Energy Frontier Research Center, Molten Salts in Extreme Environments, Chemistry Division, Brookhaven National Laboratory, Upton, New York 11973-5000, USA
[z]E-mail: vishnu@unizwa.edu.om

studies were performed to examine their oxidation behaviors and thus their possible operating temperatures in a device.

Experimental

Preparation and electrochemical processing of the sintered oxides.—The as-received Ta_2O_5 and Nb_2O_5 powders, as specified in Table S1 (Supplementary Information (SI) is available online at stacks.iop.org/JES/167/022504/mmedia) were weighed in the required proportions for the targeted alloy compositions of Ta-20Nb, Ta-50Nb and Ta-80Nb, with the numbers indicating the mass percentages of Nb in the final Ta-Nb alloys. Each oxide mixture had 1 mass% of polyvinyl alcohol and 0.5 mass% of polyethylene glycol added to it as binder/plasticizer, and the mixture was ball-milled in isopropanol for 12 h. The wet mass was then transferred into a mortar and subjected to three process cycles of drying in an oven at 80 °C, cooling in air, and re-grinding with a pestle in isopropanol; which was finally followed by drying in air. Portions of 1 to 5 g of dried powder were uniaxially pressed at an applied load of 1.5 t into a mixed oxide disk of diameter 25 mm. All disks were sintered at 1100 °C in air for 3 h. The individual oxides of Ta_2O_5 and Nb_2O_5, used for comparison, were made into pure oxide disks applying the same procedure.

About 500 g of anhydrous $CaCl_2$ salt, prepared from $CaCl_2·2H_2O$ (98+%, Sigma Aldrich) via thermal and vacuum drying,[37] was filled into an alumina crucible. This was placed inside an Inconel high-temperature reactor that was sealed leak-tight with a steel lid that had feedthroughs for the various cell components. The reactor assembly was heated to the operating temperature of 900 °C at a rate of 5 °C min^{-1} under a constant flow of argon. The salt melt was pre-electrolyzed to remove any redox-active impurities using a Ni coil cathode and a graphite rod anode, both attached to stainless steel rods as current collectors. A potential of 2.8 V was applied for several hours until a small stable background current was attained. For the electro-deoxidation experiments, the Ni cathode was replaced with an oxide disk prepared as described above. The disk was tied with Ta wire and connected to a stainless steel current collector. Also added was a Ni/NiO reference electrode to monitor the individual potentials of the cathode and the anode.[33] A potential of 3.1 V was applied between the oxide cathode and the graphite anode for 3 to 25 h. After that the electrodes were lifted above the melt and the reactor was cooled. The processed products were recovered by washing with distilled water, 0.1 M aqueous HCl, and again distilled water, until free from salt, and then dried in vacuum at ambient temperature.

The oxide disk precursors and the processed products were analyzed for phase composition, morphology and chemical composition, by means of X-ray diffraction (XRD) (Philips PW 1830), using Cu K$_\alpha$ radiation, and scanning electron microscopy (SEM) (FEI Nova NanoSEM 450), using secondary and back-scattered electrons, in combination with energy-dispersive X-ray spectroscopy (EDX) (Bruker X Flash 6I100). Open porosities of the sintered oxides were determined using the Archimedes method in distilled water. Residual oxygen contents of the processed products were measured in triplicate using the inert gas fusion method (ELTRA ONH 2000) and averaged. Some products were analyzed further by X-ray photoelectron spectroscopy (XPS) (K-alpha, Thermo VG).

Electrochemical and oxidation studies of the metallic products.—The Ta-Nb alloys as well as the Ta and Nb metals, all made as described above, were subjected to electrochemical characterization in aqueous solution by cyclic voltammetry. Working electrodes were prepared by making a slurry with mortar and pestle that contained 60 mass% of the active metallic material in powder form, 30 mass% of carbon black, and 10 mass% of polyvinylidene fluoride (PVDF) dissolved in N-methylpyrrolidone (NMP). The slurry was applied as a thin uniform coating on a Ti foil and dried in an oven at 100 °C for 12 h. The Ti foil was weighed before and after coating to evaluate the mass of active material. Measurements were conducted in a three-terminal cell,

consisting of a working electrode of the above type, Ag/AgCl and Pt foil as the reference and counter electrodes, and 1.0 M Na_2SO_4 aqueous solution as the electrolyte. Scans were recorded within a potential window of 0.0–0.8 V vs the reference at a rate of 20 mV s^{-1} at room temperature using a potentiostat (IviumStat, Ivium Technologies).

The effect of temperature on selected samples in air was investigated by means of a simultaneous thermogravimetric and differential scanning calorimetric analyzer (STA) (Netzsch STA 409 EP). About 30 mg of material was employed in each experiment, and the temperature was ramped from 25 °C–1000 °C at a rate of 20 °C min^{-1} in air.

Results and discussion

Characterization of the sintered oxides.—The XRD analysis of the sintered oxide precursor disks is compiled in Figs. 1a–1e. The patterns show the peaks of pure Ta_2O_5 and Nb_2O_5, and thus indicate that there was no reaction between them towards any ternary Ta-Nb-O compounds. The precursor for Ta-20Nb did not have any Nb_2O_5 peaks, suggesting that there is appreciable solubility of Nb_2O_5 in Ta_2O_5. The precursors for Ta-50Nb and Ta-80Nb clearly showed Ta_2O_5 and Nb_2O_5 peaks, the latter case indicating that the solubility of Ta_2O_5 in Nb_2O_5 is lower than in the reciprocal case.
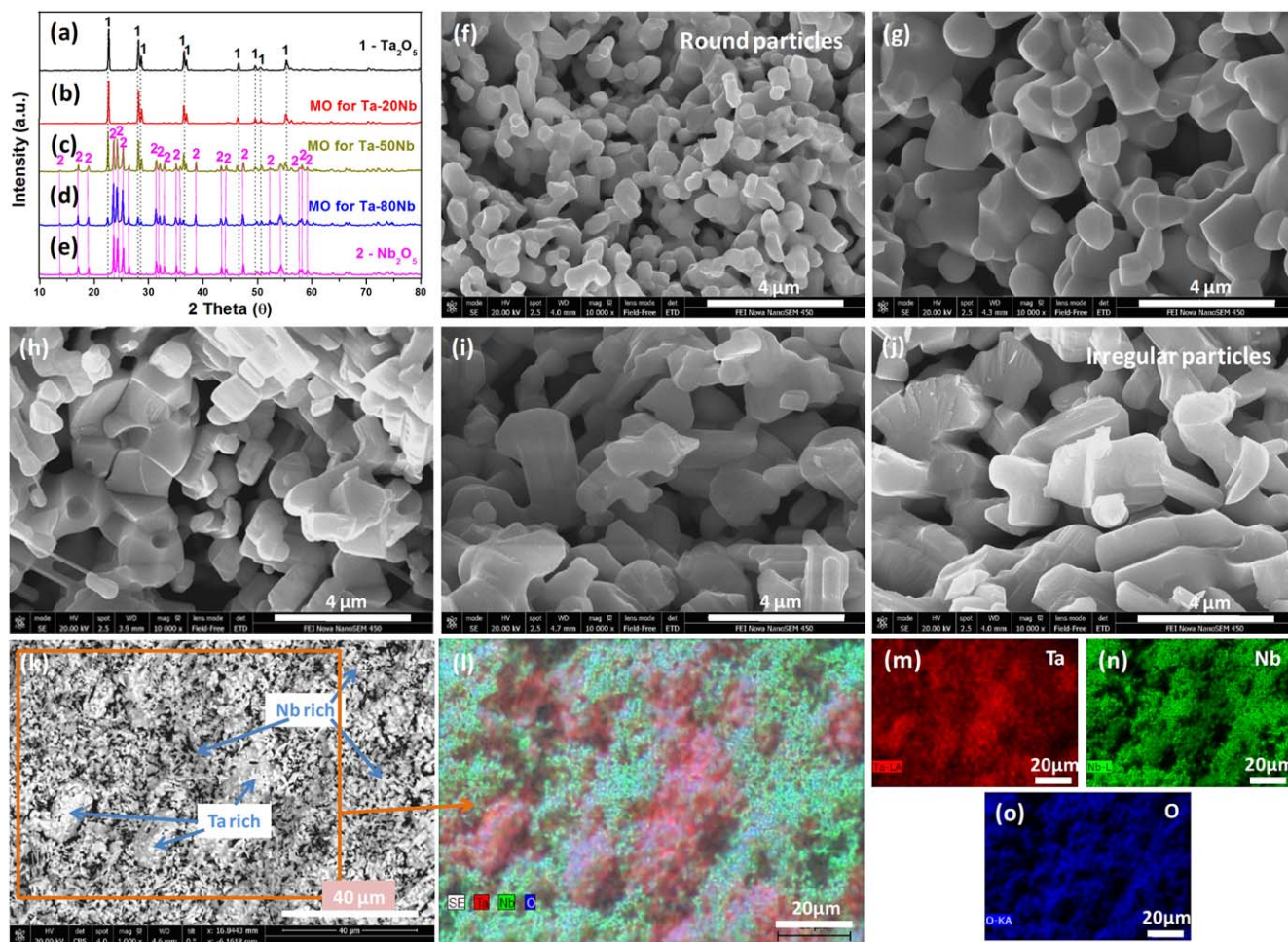
SEM images of the cross-sections of the sintered oxide precursor disks are displayed in Figs. 1f–1j. Pure Ta_2O_5 consisted of rather spherical particles in the size range of 200 nm to around 1 μm, while pure Nb_2O_5 had more irregularly shaped and somewhat larger particles in the size range of 1–5 μm. The mixed oxide precursors had particle sizes that were in between those of pure Ta_2O_5 and pure Nb_2O_5 and increased with rising Nb_2O_5 content in the Ta_2O_5, with visually distinguishable round and jagged particles present in all cases (Fig. S1). It was noticed that in the case of the precursor for Ta-20Nb, although particle size had increased, the shape of most of the particles still resembled that in Ta_2O_5, in line with the notion of high solubility of Nb_2O_5 in Ta_2O_5 as suggested by the X-ray analysis. It is moreover discernible from the microstructures that all the samples contained a significant number of pores, which is helpful for enhancing molten salt penetration.

The EDX analysis of the cross-section of the sintered oxide precursor for Ta-50Nb is presented in Fig. 1k–1o. It is observed that the distribution of Ta and Nb was largely random with slight local variations in some regions. However, for precursors with lower contents of Ta_2O_5, a small but noticeable extent of Ta_2O_5 segregation into regions of several tens of micrometers in size could be seen on back-scattered SEM images (Figs. S2, S3).

The open porosities of the sintered oxide precursors were in the range of 41%–55% (Table S2, Fig. S4). The general tendencies were that both the open porosity and the density of the oxides decreased with increasing Nb_2O_5 content, with some deviation for the precursor for Ta-20Nb. Ta_2O_5 has a higher melting temperature than Nb_2O_5 (Table S1) and will therefore densify less during sintering and that will also have an effect on the mixed oxides. The observed deviation may be a result of the assumed significant chemical solubility of Nb_2O_5 in Ta_2O_5.

Electrochemical processing of the sintered oxides.—The current vs time curves recorded during the electro-deoxidation of the sintered Ta_2O_5-Nb_2O_5 mixed oxide disks, as well as those of the pure oxide disks of Ta_2O_5 and Nb_2O_5, are presented in Fig. 2a, and the corresponding cathodic potential vs time curves are shown in Fig. 2b. The processed products were found to be gray colored powders, in contrast to the oxide precursors that were white colored disks, as seen from Figs. 2c–2m, indicating the successful conversion of oxidic into metallic materials.

The variation of the current with time showed similar features for all oxide samples. The high initial currents on the order of 2.5–3.5 A indicated that the oxides had significant porosity, providing a high active surface area in the beginning, and good electronic conduction. The currents during the first 2 h are presented in the inset of Fig. 2a.

Figure 1. X-ray patterns of metal oxide (MO) disks of (a) Ta_2O_5, (b) precursor for Ta-20Nb, (c) precursor for Ta-50Nb, (d) precursor for Ta-80Nb, and (e) Nb_2O_5, all sintered at 1100 °C in air for 3 h. SEM images of the cross-sections of the same disks of (f) Ta_2O_5, (g) precursor for Ta-20Nb, (h) precursor for Ta-50Nb, (i) precursor for Ta-80Nb, and (j) Nb_2O_5. (k) Low-magnification SEM image of precursor for Ta-50Nb, with (l) survey EDX elemental map, and individual EDX elemental maps for (m) Ta, (n) Nb, and (o) O.

They increased in the order of Ta < Ta-20Nb < Ta-50Nb < Ta-80Nb < Nb. Ta_2O_5 is thermodynamically more stable than Nb_2O_5 (Table S3) and thus requires more energy for undergoing dissociation. As the applied voltage was the same in all cases, there was thus a higher overpotential available for the reaction of Nb_2O_5 that could drive a comparatively higher current. After the initial period, currents decayed and then stabilized during the remainder of the runs at relatively low values around 400–800 mA.

The cathodic potentials corresponding to the high currents during the first 2 h were within the range of 0.75–0.40 V vs Ca/Ca^{2+}, after that they assumed smaller but still positive values. The relatively high positive potentials in the beginning were indicative of the occurrence of less energy-demanding reactions, such as the formation of M-Ca-O compounds (M = Ta and Nb) and Ta- and Nb-suboxides that had been seen previously in the individual electro-deoxidations of Ta_2O_5 and Nb_2O_5. The potentials became less positive when more energy-demanding reactions set in, driving the release of Ta and Nb from the various intermediates. Importantly, the cathodic potentials never went into the negative, proving that no calcium deposition occurred at any stage of the process. Current efficiencies were in the range of 18%–42%, and decreased with increasing process duration as is common for this method, with the current loss being mainly due to the intrinsic electronic conductivity of the polarized melt.[18]

Characterization of the metallic products.—XRD analysis.—
The XRD analysis of the processed products is compiled in Figs. 3a–3e.

The patterns of the pure metal powders of Ta and Nb as well as those of the alloy powders of Ta-20Nb, Ta-50Nb and Ta-80Nb were all practically identical, showing a single-phase body-centered cubic structure. The absence of any additional peaks indicated that the materials were devoid of any Ca-Ta-Nb-O or other impurity phases. It is noted that all XRD data reported in the literature for Ta and Nb prepared in $CaCl_2$ melt showed the cubic structure. In contrast, Ta made in LiCl melt was either tetragonal or a mix of cubic and tetragonal,[22] whereas Nb made in LiCl was again cubic.[31]

SEM/EDX and residual oxygen analysis.—SEM images of the processed products are displayed in Figs. 3f–3j. The Ta and Nb metal powders were of uniform nodular morphology with loosely interconnected particles, with the particle size of the Ta in the size range of 100–800 nm and the Nb in the somewhat larger size range of 200 nm to several micrometers. The smaller particle size of Ta was consequent of a lower degree of *in situ* sintering compared with that of Nb due to their vastly different melting points (Table S1). The Ta-20Nb alloy powder also had a uniform nodular morphology with particles of similar size as in the Ta powder, whereas the Ta-50Nb and the Ta-80Nb alloy powders had bimodal morphologies, with smaller nodular and bigger spherical particles (Fig. S5).

The EDX analysis of the synthesized Ta-50Nb alloy powder is presented in Figs. 3k–3o. This shows that all particles contained Ta and Nb and that the particles of smaller size were enriched with Ta and those of bigger size with Nb (Fig. S6). The elemental compositions of all materials prepared, as estimated by EDX area
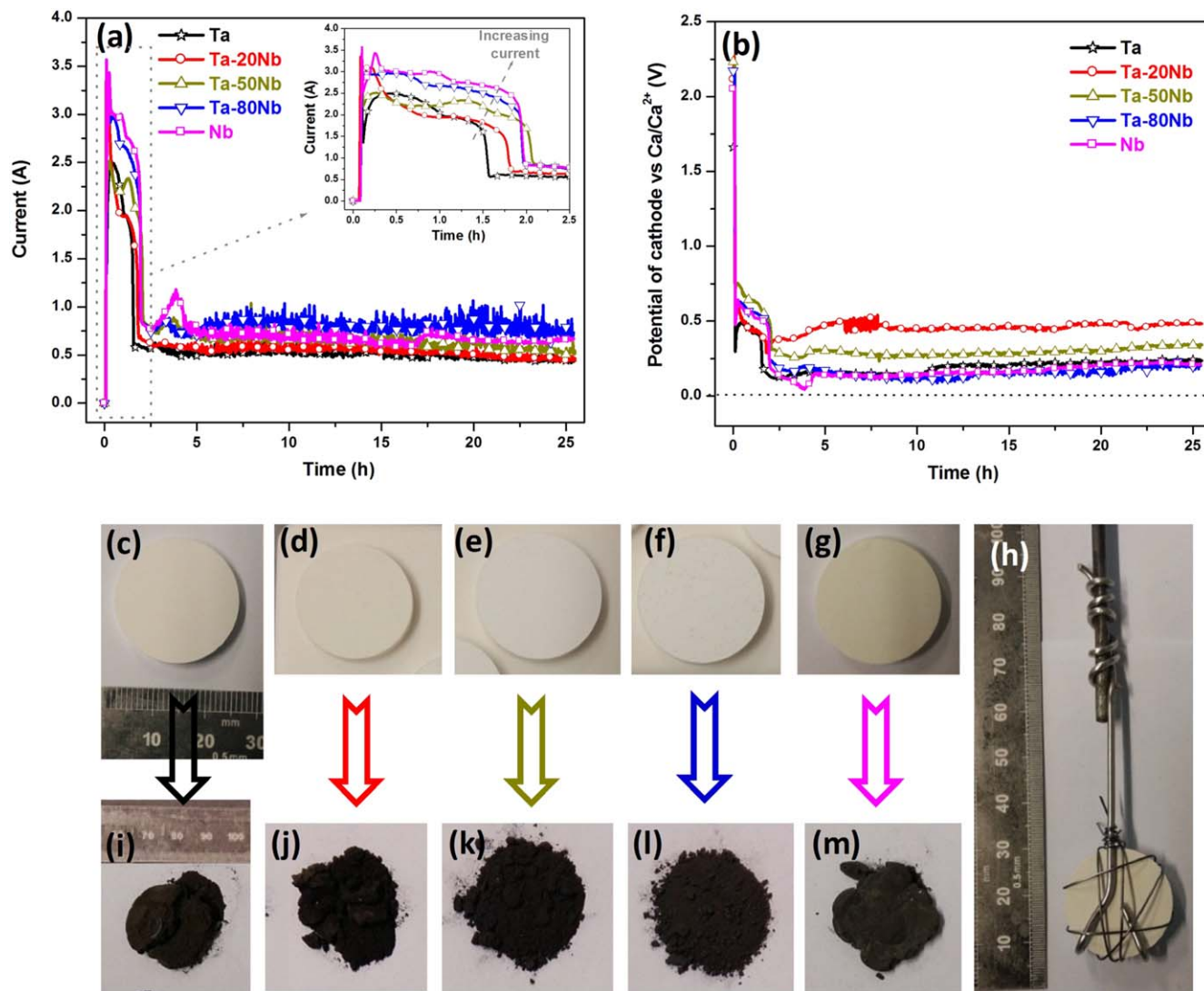
Figure 2. (a) Current vs time curves and (b) cathodic potential vs time curves, recorded during the electro-deoxidation of pure and mixed oxide precursor disks, each of 5.0 g in mass and 25 mm in diameter, employed as the cathode against a graphite anode in $CaCl_2$ melt at 900 °C and 3.1 V for 25 h. Photographs of oxide precursor disks for (c) Ta, (d) Ta-20Nb, (e) Ta-50Nb, (f) Ta-80Nb, and (g) Nb; (h) the typical configuration of cathode before electro-deoxidation; and (i-m) the respective metal or alloy powders after electro-deoxidation.

scans, are summarized in Table I. Importantly, the EDX analysis gave oxygen contents of about 3% in each case. The presence of oxygen was indeed expected, because the freshly prepared metallic materials of high specific surface area will invariably undergo surface reactions in the washing steps with water and diluted HCl to form thin oxide films. Similar to the present study, Wu et al.[30] reported that the EDX analysis of Nb made in $CaCl_2$ melt gave an oxygen content of 3.27%. TEM analysis of Ta and Nb made in molten salts revealed that the surface oxide films were around 2–5 nm thick in the case of Ta[21] and 4–6 nm in the case of Nb.[30]

Inert gas fusion analysis yielded a residual oxygen content of 1.3% for the Ta-50Nb alloy powder and thus a significantly lower value compared with the EDX analysis. The difference is understandable because EDX predominantly measures the surface oxygen content whereas inert gas fusion measures the total oxygen content. In line with this, Yan and Fray reported a total residual oxygen content for Nb made in $CaCl_2$ melt of about 1%[26] and Wu et al. of 1.5%.[30]

XPS analysis.—The XPS survey spectrum of the Ta-50Nb alloy powder is shown in Fig. 4a. It comprises exclusively the peaks for

Ta, Nb and O. The high-resolution spectra for Ta (Ta4f), Nb (Nb3d) and O (O1s) are shown in Figs. 4b–4d. For Ta, the peaks at 26.1 and 27.9 eV correspond to the $4f_{7/2}$ and $4f_{5/2}$ levels of Ta_2O_5 and those at 21.0 and 22.8 eV to the $4f_{7/2}$ and $4f_{5/2}$ levels of Ta metal.[38–40] For Nb, the high-intensity peaks at 207.1 and 209.9 eV stem from the $3d_{5/2}$ and $3d_{3/2}$ levels of Nb_2O_5 and the low-intensity peaks at 201.7 and 204.8 eV from the $3d_{5/2}$ and $3d_{3/2}$ levels of Nb metal.[38,39] For

Table I. Chemical composition of the metal and alloy powders synthesized by electro-deoxidation of pure and mixed oxide precursor disks in $CaCl_2$ melt at 900 °C and 3.1 V for 25 h.

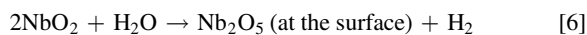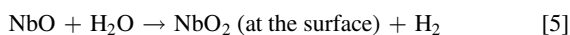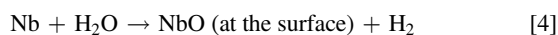| Metal/alloy product	Composition (mass%)		
	Ta	Nb	O
Ta	96.8	—	3.2
Ta-20Nb	81.0	15.5	3.5
Ta-50Nb	54.1	42.9	3.1
Ta-80Nb	36.6	60.2	3.2
Nb	—	96.8	3.2
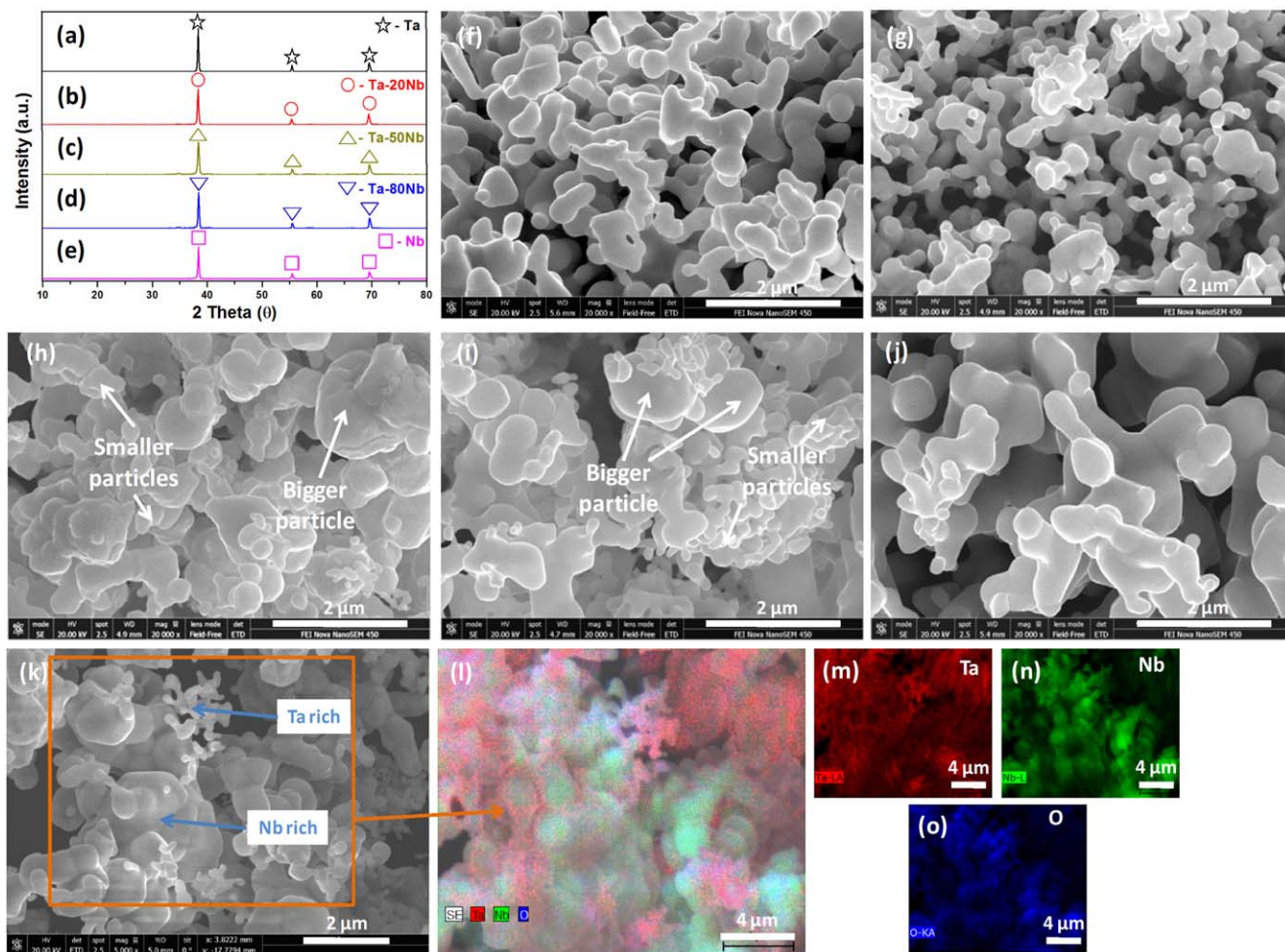
Figure 3. X-ray patterns of product powders of (a) Ta, (b) Ta-20Nb, (c) Ta-50Nb, (d) Ta-80Nb, and (e) Nb, all obtained by electro-deoxidation. SEM images of the products of (f) Ta, (g) Ta-20Nb, (h) Ta-50Nb, (i) Ta-80Nb, and (j) Nb. (k) SEM image of another region of Ta-50Nb, with (l) survey EDX elemental map, and individual EDX elemental maps for (m) Ta, (n) Nb, and (o) O.

oxygen, the hump peaking at around 530.3 eV can be attributed to the $1s$ level of O^{2-} ions, and the broad shoulder at slightly higher energy to the $1s$ level in adsorbed H_2O.[38] Overall, the results demonstrate that Ta and Nb occur in their highest, pentavalent, oxidation states in the oxide film on top of the alloy bulk, with no detectable amounts in any intermediate oxidation state.

It is straightforward to assume that the highly reactive nature of the electrochemically synthesized Ta-Nb alloy powders has thus enabled the following sequences of surface reactions when in contact with water.

$$Ta + H_2O \rightarrow TaO \text{ (at the surface)} + H_2 \qquad [1]$$

$$TaO + H_2O \rightarrow TaO_2 \text{ (at the surface)} + H_2 \qquad [2]$$

$$2TaO_2 + H_2O \rightarrow Ta_2O_5 \text{ (at the surface)} + H_2 \qquad [3]$$

$$Nb + H_2O \rightarrow NbO \text{ (at the surface)} + H_2 \qquad [4]$$

$$NbO + H_2O \rightarrow NbO_2 \text{ (at the surface)} + H_2 \qquad [5]$$

$$2NbO_2 + H_2O \rightarrow Nb_2O_5 \text{ (at the surface)} + H_2 \qquad [6]$$
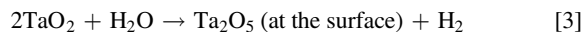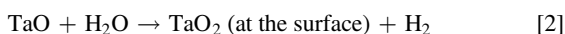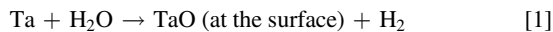
Electrochemical characterization of the metallic products.—
The cyclic voltammograms recorded to assess the electrochemical

behavior of the synthesized Ta-Nb alloy powders as well as the Ta and Nb metal powders in aqueous solution are seen in Fig. 5. Ta provided a rectangular response as is typical of capacitor materials. The shape of the curves did not change significantly when the Ta was replaced successively with Nb, indicating that the Ta-Nb alloy powders and the pure Nb powder also acted as capacitors. There is no direct correlation between the composition of the working electrodes and the magnitude of the currents, so it may be assumed that the small differences between the individual curves resulted from some fluctuations in the preparation and testing of the electrodes. The quest for a facile method for the making of Ta-Nb powders for use in capacitors[8] has thus been solved, but it will of course need to be tested by the relevant industries what the maximum level of Nb is that can finally be tolerated in commercial devices.

Oxidation studies of Ta and Ta-50Nb alloy.—The STA curves obtained for Ta and Ta-50Nb powders in air are displayed in Figs. 6a, 6b. For both materials a slow but noticeable increase in mass started at around 300 °C. In the case of Ta a steep mass increase was then observed from 531 °C–562 °C, leading to a net gain of 20 mass%, and in the case of Ta-50Nb such increase was seen from 363 °C–422 °C, causing a gain of 28 mass%. For Ta the mass continued to increase linearly up to 700 °C, followed by a
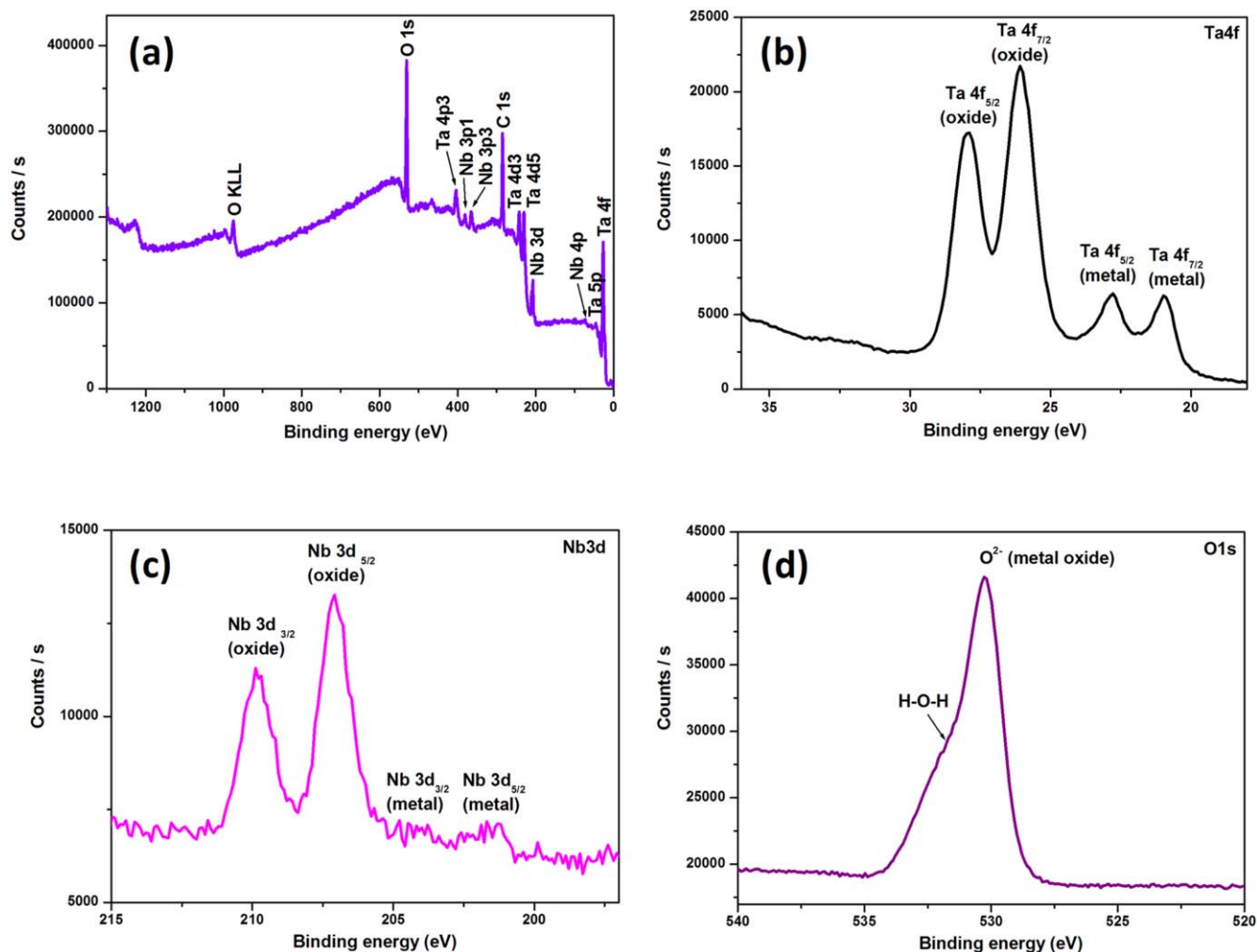
Figure 4. X-ray photoelectron spectroscopic analysis of Ta-50Nb alloy, with (a) XPS survey spectrum, and XPS high-resolution spectra for (b) Ta, (c) Nb, and (d) O.

very small rise up to 1000 °C. For Ta-50Nb however the mass increased only up to 650 °C, but then dropped back and rose only marginally beyond that.
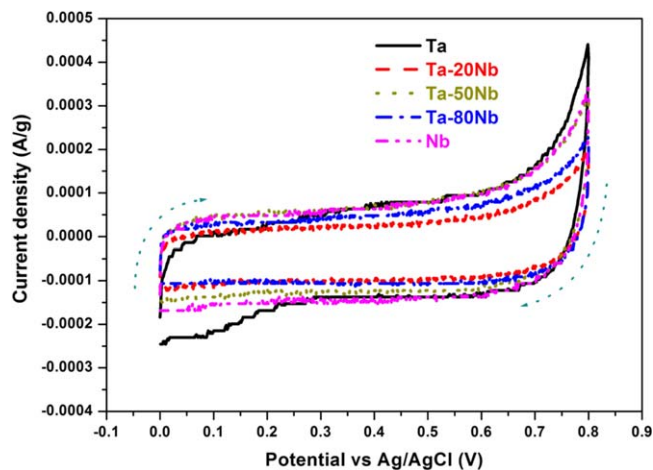

Figure 5. Electrochemical analysis by cyclic voltammetry of Ta, Ta-Nb alloys, and Nb in 1 M Na_2SO_4 aqueous solution, with Ag/AgCl as the reference and platinum as the counter electrodes, at a scan rate of 20 mV s^{-1} at 25 °C.

The initial sluggish mass gains in the TGA curves were indicative of slow diffusion of oxygen through the oxide barrier at the surface of the particles towards the bulk where a solid solution of oxygen in the metal is formed.[41] It was reported that this can lead to oxygen supersaturation and embrittlement.[42] The subsequent steep mass gains were then due to oxidation reactions, as indicated by the highly exothermic nature of the corresponding sections of the DSC scans. The oxidation temperature of Ta-50Nb was lower than that of Ta. This is attributed to the presence of Nb in the former, which is known to have a higher oxidation tendency than Ta.[43] It has further been reported that the spallation of the surface oxide layer occurs more rapidly on Nb than on Ta,[43] so this may also have contributed to the earlier start of oxidation for Ta-50Nb.

The abrupt mass loss in the TGA curve for Ta-50Nb observed at 650 °C is a peculiar phenomenon associated with the inversion of the temperature coefficient of the oxidation reaction. It is known from the oxidation of pure Nb,[42,44–46] where the mass during oxidation increases up to 635 °C and then drops with further rise in temperature owing to changes in the nature of the oxide film. Such inversion was also reported for Nb-V alloy,[46] but has not been reported for Ta.

After the STA experiments, the originally metallic gray powders had turned white and had gained in mass. Quantitatively, the oxidation of Ta metal to its pentavalent oxide was found to be complete, whereas this was indeed not the case for the Ta-50Nb alloy. In a typical run with the latter, the mass had increased from its initial value of 30.6 mg to a final value of only 38.6 mg while total oxidation would have led to 40.6 mg.
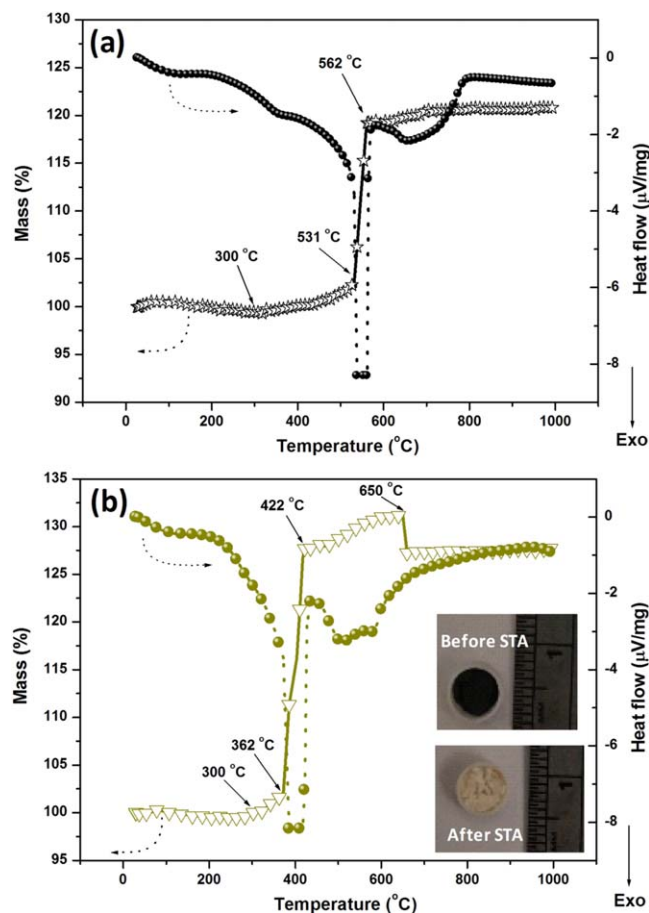
Figure 6. Simultaneous thermogravimetric and differential scanning calorimetric analysis (STA) of (a) Ta and (b) Ta-50Nb alloy, when heated from ambient temperature to 1000 °C in air at 20 °C min^{-1}. Inset in (b) shows photographs of Ta-50Nb before and after STA.

Conclusions

The study has demonstrated that Ta-xNb alloys (x = 20, 50, 80) can be readily prepared from the corresponding mixed oxides by electro-deoxidation in CaCl$_2$ melt. XRD analysis of the oxides showed that co-sintering of Ta$_2$O$_5$ and Nb$_2$O$_5$ did not lead to the formation of any compounds while the absence of peaks for Nb$_2$O$_5$ in the mixed oxide for Ta-20Nb indicated appreciable solubility of Nb$_2$O$_5$ in Ta$_2$O$_5$. The Ta-Nb alloys synthesized, as well as the pure Ta and Nb metals prepared analogously, were all in the form of powders. XRD analysis of the products confirmed that the materials were phase pure and had the expected body-centered cubic structure. SEM analysis showed that particle size increased with increasing Nb content, from a few hundred nanometers for pure Ta and Ta-20Nb to several micrometers for pure Nb. Ta-50Nb and Ta-80Nb had particles of two different size ranges, the smaller ones enriched with Ta and the bigger ones enriched with Nb.

Both EDX and inert gas fusion studies of the products revealed the presence of a small percentage of residual oxygen. XPS studies further identified the presence of a thin surface oxide film around the particles. Surface oxidation occurred during washing with water subsequent to electro-deoxidation, and is thus the key step in the formation of the dielectric film around the metallic core. Cyclic voltammetry confirmed that the Ta, Ta-Nb and Nb powders all exhibited capacitive performance. STA studies in air identified the highest operating temperature of the materials as approximately 300 °C, whereafter significant oxidation set in. STA further revealed an inversion in the temperature coefficient of the oxidation for Ta-50Nb at 650 °C.

In overall, the molten salt electro-deoxidation method is a facile and straightforward, and known to be scalable, way of producing Ta-Nb alloys for electrolytic capacitors. Several aspects ought to be considered in the further development of this research. One target would be the optimization of the surface oxide layer. If the oxygen content needs to be lowered, this may be accomplished by using less reactive solvents, such as ethanol, in the washing step after reduction; while if the oxygen content needs to be increased, this may be achieved in a controlled manner by anodization. Another objective could be to operate in a carbon-free electrochemical cell. This may be ensured through the utilization of non-carbon anodes, such as doped SnO$_2$ or CaTi$_x$Ru$_{1-x}$O$_3$, as presently researched.[18] Finally, even smaller product particle sizes should be attainable by using finer oxide powders as the starting materials, ideally in combination with lower temperatures in the electro-deoxidation so as to minimize *in situ* sintering even further.

References

1. S. M. Cardonne, P. Kumar, C. A. Michaluk, and H. D. Schwartz, "Tantalum and its alloys." *Int. J. Refr. Metals Hard Mater.*, **13**, 187 (1995).
2. A. Robin, "Corrosion behavior of niobium, tantalum and their alloys in boiling sulfuric acid solutions." *Int. J. Refr. Metals Hard Mater.*, **15**, 317 (1997).
3. A. Robin and J. L. Rosa, "Corrosion behavior of niobium, tantalum and their alloys in hot hydrochloric and phosphoric acid solutions." *Int. J. Refr. Metals Hard Mater.*, **18**, 13 (2000).
4. N. Kobayashi, K. Noto, M. Ikebe, and Y. Muto, "Thermal conductivity of Ta-Nb alloys in superconducting, mixed, and normal states." *J. Low Temp. Phys.*, **17**, 575 (1974).
5. H. F. Wang, J. Li, H. L. Yang, C. Liu, and J. M. Ruan, "Fabrication, characterization and in vitro biocompatibility evaluation of porous Ta-Nb alloy for bone tissue engineering." *Mater. Sci. Eng. C*, **40**, 71 (2014).
6. J. M. Sanz and S. Hofmann, "Auger electron spectroscopy and X-ray photoelectron spectroscopy studies of the oxidation of polycrystalline tantalum and niobium at room temperature and low oxygen pressures." *J. Less Common Met.*, **92**, 317 (1983).
7. A. Michaelis, "Valve metal, Si and ceramic oxides as dielectric films for passive and active electronic devices." in *Advances in Electrochemical Science and Engineering*, ed. R. C. Alkire et al. (Wiley-VCH, Weinheim, Germany) Vol. 10 Chap. 1, p. 1 (2008).
8. Y. Freeman, *Tantalum and Niobium-Based Capacitors: Science, Technology, and Applications* (Springer, Cham, Switzerland) (2018).
9. G. L. Miller, *Tantalum and Niobium* (Butterworths Scientific, London, UK) (1959).
10. C. K. Gupta, "Extractive metallurgy of niobium, tantalum, and vanadium." *Int. Met. Rev.*, **29**, 405 (1984).
11. C. A. Nunes, D. G. Pinatti, and A. Robin, "Nb-Ta alloys by aluminothermic reduction of Nb$_2$O$_5$/Ta$_2$O$_5$ mixtures and electron beam melting." *Int. J. Refr. Metals Hard Mater.*, **17**, 305 (1999).
12. A. Awasthi, Y. J. Bhatt, N. Krishnamurthy, Y. Ueda, and S. P. Garg, "The reduction of niobium and tantalum pentoxides by silicon in vacuum." *J. Alloys Compd.*, **315**, 187 (2001).
13. K. C. Gandolpho Candioto and C. A. Nunes, "Nb-20%Ta alloy powder by the hydriding-dehydriding technique." *Int. J. Refr. Metals Hard Mater.*, **24**, 413 (2006).
14. G. Z. Chen, D. J. Fray, and T. W. Farthing, "Direct electrochemical reduction of titanium dioxide to titanium in molten calcium chloride." *Nature*, **407**, 361 (2000).
15. D. J. Fray, "Novel methods for the production of titanium." *Int. Mater. Rev.*, **53**, 317 (2008).
16. D. H. Wang, X. B. Jin, and G. Z. Chen, "Solid state reactions: an electrochemical approach in molten salts." *Annu. Rep. Prog. Chem. Sect. C*, **104**, 189 (2008).
17. K. S. Mohandas, "Direct electrochemical conversion of metal oxides to metal by molten salt electrolysis: a review." *Miner. Proc. Extract. Metall.*, **122**, 195 (2013).
18. D. J. Fray and C. Schwandt, "Aspects of the application of electrochemistry to the extraction of titanium and its applications." *Mater. Trans.*, **58**, 306 (2017).
19. R. O. Suzuki, K. Ono, and K. Teranuma, "Calciothermic reduction of titanium oxide and in-situ electrolysis in molten CaCl$_2$." *Metall. Mater. Trans. B*, **34**, 287 (2003).
20. R. O. Suzuki, "Direct reduction processes for titanium oxide in molten salt." *JOM*, **59**, 69 (2007).
21. T. Wu, X. B. Jin, W. Xiao, X. H. Hu, D. H. Wang, and G. Z. Chen, "Thin pellets: fast electrochemical preparation of capacitor tantalum powders." *Chem. Mater.*, **19**, 153 (2007).

22. S. M. Jeong, J. Y. Jung, C. S. Seo, and S. W. Park, "Characteristics of an electrochemical reduction of Ta_2O_5 for the preparation of metallic tantalum in a LiCl-Li_2O molten salt." *J. Alloys Compd.*, **440**, 210 (2007).
23. R. Barnett, K. T. Kilby, and D. J. Fray, "Reduction of tantalum pentoxide using graphite and tin-oxide-based anodes via the FFC-Cambridge process." *Metall. Mater. Trans. B*, **40**, 150 (2009).
24. Q. S. Song, Q. Xu, X. Kang, J. H. Du, and Z. P. Xi, "Mechanistic insight of electrochemical reduction of Ta_2O_5 to tantalum in a eutectic $CaCl_2$-NaCl molten salt." *J. Alloys Compd.*, **490**, 241 (2010).
25. X. Y. Yan and D. J. Fray, "Production of niobium powder by direct electrochemical reduction of solid Nb_2O_5 in a eutectic $CaCl_2$-NaCl melt." *Metall. Mater. Trans. B*, **33**, 685 (2002).
26. X. Y. Yan and D. J. Fray, "Electrochemical studies on reduction of solid Nb_2O_5 in molten $CaCl_2$-NaCl eutectic: I. Factors affecting electrodeoxidation of solid Nb_2O_5 to niobium." *J. Electrochem. Soc.*, **152**, D12 (2005).
27. X. Y. Yan and D. J. Fray, "Electrochemical studies on reduction of solid Nb_2O_5 in molten $CaCl_2$-NaCl eutectic: II. Cathodic processes in electrodeoxidation of solid Nb_2O_5." *J. Electrochem. Soc.*, **152**, E308 (2005).
28. Q. Xu, L. Q. Deng, Y. Wu, and T. Ma, "A study of cathode improvement for electro-deoxidation of Nb_2O_5 in a eutectic $CaCl_2$-NaCl melt at 1073 K." *J. Alloys Compd.*, **396**, 288 (2005).
29. S. L. Wang, Y. Xue, and H. Sun, "Electrochemical study on the electrodeoxidation of Nb_2O_5 in equimolar $CaCl_2$ and NaCl melt." *J. Electroanal. Chem.*, **595**, 109 (2006).
30. T. Wu, W. Xiao, X. B. Jin, C. Liu, D. H. Wang, and G. Z. Chen, "Computer-aided control of electrolysis of solid Nb_2O_5 in molten $CaCl_2$." *Phys. Chem. Chem. Phys.*, **10**, 1809 (2008).
31. S. M. Jeong, H. Y. Yoo, J. M. Hur, and C. S. Seo, "Preparation of metallic niobium from niobium pentoxide by an indirect electrochemical reduction in a LiCl-Li_2O molten salt." *J. Alloys Compd.*, **452**, 27 (2008).
32. Q. S. Song, Q. Xu, R. Tao, and X. Kang, "Cathodic phase transformations during direct electrolytic reduction of Nb_2O_5 in a $CaCl_2$-NaCl-CaO melt." *Int. J. Electrochem. Sci.*, **7**, 272 (2012).
33. D. S. M. Vishnu, N. Sanil, L. Shakila, G. Panneerselvam, R. Sudha, K. S. Mohandas, and K. Nagarajan, "A study of the reaction pathways during electrochemical reduction of dense Nb_2O_5 pellets in molten $CaCl_2$ medium." *Electrochim. Acta*, **100**, 51 (2013).
34. M. Baba and R. O. Suzuki, "Dielectric properties of tantalum powder with broccoli-like morphology." *J. Alloys Compd.*, **392**, 225 (2005).
35. Y. T. Yuan, W. Li, H. L. Chen, Z. Y. Wang, X. B. Jin, and G. Z. Chen, "Electrolysis of metal oxides in $MgCl_2$ based molten salts with an inert graphite anode." *Faraday Discuss.*, **190**, 85 (2016).
36. Q. Xu, C. Schwandt, and D. J. Fray, "Preparation of Ta-Nb alloy powder by electro-deoxidation of Ta_2O_5/Nb_2O_5 mixture in a $CaCl_2$-NaCl eutectic melt." *Adv. Mater. Res.*, **160–162**, 1131 (2011).
37. D. S. M. Vishnu, J. Sure, H.-K. Kim, J.-Y. Kim, R. V. Kumar, and C. Schwandt, "Direct electrochemical preparation of nanostructured silicon carbide and its nitridation behavior." *J. Electrochem. Soc.*, **165**, D731 (2018).
38. J. F. Moulder, W. F. Stickle, P. E. Sobol, and K. D. Bomben, *Handbook of X-ray Photoelectron Spectroscopy* (Perkin-Elmer Corporation, Eden Prairie, MN) (1992).
39. C. D. Wagner, J. W. Allison, J. R. Rumble Jr, A. V. Naumkin, A. Kraut-Vass, and C. J. Powell, X-ray Photoelectron Spectroscopy Database, Version 3.0-3.4, National Institute of Standards and Technology NIST, Gaithersburg, MD [http://srdata.nist.gov/xps/main_search_menu.aspx] (2000–2003).
40. J. Jayaraj, C. Thinaharan, S. Ningshen, C. Mallika, and U. Kamachi Mudali, "Corrosion behavior and surface film characterization of TaNbHfZrTi high entropy alloy in aggressive nitric acid medium." *Intermetallics*, **89**, 123 (2017).
41. D. A. Vermilyea, "The oxidation of tantalum at 50–300°C." *Acta Metall.*, **6**, 166 (1958).
42. J. S. Sheasby, "The oxidation of niobium in the temperature range 450°–720°C." *J. Electrochem. Soc.*, **115**, 695 (1968).
43. I. McKee and G. R. Wallwork, "The oxidation of tantalum and niobium in the temperature range 400°–600°C." *J. Less Common Met.*, **30**, 249 (1973).
44. D. W. Bridges and W. M. Fassell Jr, "High pressure oxidation of niobium." *J. Electrochem. Soc.*, **103**, 326 (1956).
45. D. W. Aylmore, S. J. Gregg, and W. B. Jepson, "Oxidation of niobium in the temperature range 350°–750°C." *J. Electrochem. Soc.*, **107**, 495 (1960).
46. T. Mukaibo, M. Kanno, and M. Yamawaki, "Oxidation behavior of Nb and Nb-V alloys." *J. Nucl. Sci. Technol.*, **2**, 516 (1965).